Development and Validation of a Multi-zone Predictive Combustion Model for Large-Bore Dual-Fuel Engines

SAE INTERNATIONAL

ARTICLE INFO
Article ID: 03-15-05-0038

doi:10.4271/03-15-05-0038

Development and Validation of a Multi-zone Predictive Combustion Model for Large-Bore Dual-Fuel Engines

Federico Millo,[1] Francesco Accurso,[1] Andrea Piano,[1] Navin Fogla,[2] Gennaro Caputo,[3] Alberto Cafari,[4] and Jari Hyvönen[4]

[1]Politecnico di Torino, Italy
[2]Gamma Technologies LLC, USA
[3]Wärtsilä Italia S.p.A., Italy
[4]Wärtsilä Finland OY, Finland

Abstract

Numerical simulation represents a fundamental tool to support the development process of new propulsion systems. In the field of large-bore dual-fuel (DF) engines, the engine simulation by means of fast running numerical models is nowadays essential to reduce the huge effort for testing activities and speed up the development of more efficient and low-emissions propulsion systems. However, the simulation of the DF combustion by means of a zero-dimensional/one-dimensional (0D/1D) approach is particularly challenging due to the combustion process evolution from spray autoignition to turbulent flame propagation and the complex interaction between the two fuels. In this regard, in this activity a 0D/1D multi-zone DF combustion model was developed for the simulation of the combustion process in large-bore DF engines. The model combines a multi-packet approach for tracking the evolution and the autoignition of the pilot fuel with an entrainment and burn-up approach for the simulation of the premixed air-gas mixture flame propagation. To properly consider the properties of the fuels involved in the combustion process and to capture the interaction between the two fuels, the DF combustion model was optimized by developing and implementing a refined ignition delay model and specific laminar and turbulent flame speed correlations optimized for high-pressure and lean air-gas mixture. In addition to this, a multi-zone Nitrogen Oxides (NOx) model was developed and integrated into the combustion model. Experimental measurements from a single-cylinder Wärtsilä research engine were used for the model development and validation. The proposed DF combustion model is able to properly capture the effect of the main engine settings (i.e., load, pilot fuel injection strategy, compression ratio (CR), and boost pressure), providing accurate predictions of the ignition timing, combustion duration, and NOx emissions. The developed numerical model can be therefore exploited to virtually assess the potential of different engine technologies and calibration strategies.

History

Received: 21 Sep 2021
Revised: 27 Nov 2021
Accepted: 08 Dec 2021
e-Available: 22 Dec 2021

Citation

Millo, F., Accurso, F., Piano, A., Fogla, N. et al., "Development and Validation of a Multi-zone Predictive Combustion Model for Large-Bore Dual-Fuel Engines," *SAE Int. J. Engines* 15(5):2022, doi:10.4271/03-15-05-0038.

ISSN: 1946-3936
e-ISSN: 1946-3944

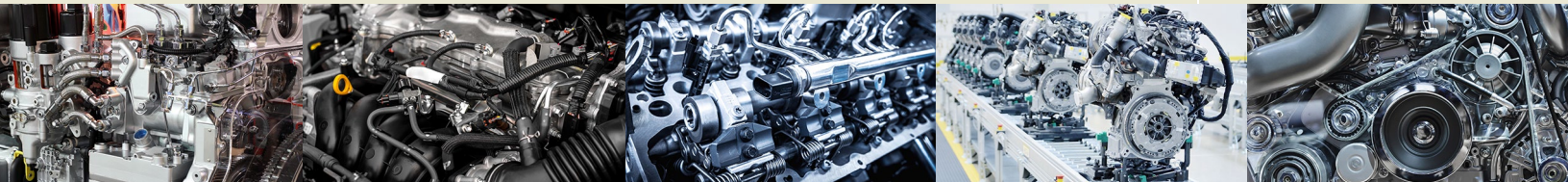

1. Introduction

The use of Liquified Natural Gas (LNG) for marine propulsion is nowadays the most effective solution to comply with current International Maritime Organization (IMO) regulations for Nitrogen Oxides (NOx) emissions [1], as well as limitations on the use of sulfur [2, 3]. In order to achieve very low NOx levels, low-temperature combustion has been widely investigated in the marine sector for years with the aim to limit the in-cylinder temperature below the activation temperatures for nitrogen oxidation. To do this, it is necessary not only to reduce the temperature at the end of the compression stroke, through advanced strategies of intake valve lift [4], but also to increase the dilution of the mixture by acting either with an air-to-fuel ratio higher than stoichiometric or with the recirculation of cooled exhaust gases [5]. However, the need to ensure good combustion stability and rapid oxidation of the fuel even in the case of lean-burn, large-bore engines requires the adoption of non-conventional ignition systems [6, 7]. In this context, Dual Fuel (DF) engines represent an established technology in the marine sector. The main idea is to trigger the propagation of the flame front through a small amount of diesel fuel that is injected during the compression stroke, exploiting the different reactivity of the two fuels. Although this technology is well established and has been in production for several years, the optimization of the combustion process requires a considerable effort to meet the upcoming and even more stringent regulations in this field. Above all, the need to reduce anthropogenic Greenhouse Gases (GHG) emissions has led in recent years to the introduction of progressive regulations also in the marine sector. Specifically, the IMO is gradually enforcing targets to reach the ambitious achievement of at least a 50% reduction of the total annual greenhouse gases volume by 2050, compared to 2008 [8]. In addition to this, the reduction of unburned hydrocarbon emissions in lean-burn gas engines is gaining even more attention among engine manufacturers [9]. Since methane (CH_4) is estimated to have a Global Warming Potential of 28-36 times greater than carbon dioxide (CO_2) [10], the disadvantages due to the emission of unburned hydrocarbons may reduce or even overcome the advantages in terms of GHG from the use of natural gas compared to marine oil fuel [11, 12].

While, from one side, the regulatory framework has a major impact on strategies and engine technologies to be investigated, other key drivers from the market have to be addressed, such as improvement of loading capability and engine efficiency in the entire engine load range, in conjunction with the continuous reduction of time-to-market for new products. However, the complexity of these propulsion systems and the large number of variables to be optimized require an impressive effort during the testing phases. Several works present in the literature confirm the great difficulties to be faced during the optimization of DF combustion [13, 14] as it is necessary to meet the emission limits having a small margin from both knock and misfire at high loads, and high instability at low loads [15], and it is also necessary to guarantee a safe operation with fuel characteristics that may vary considerably depending on the geographical area in which the engines will operate.

In view of these ambitious emission targets and challenging market needs, the engine development phase cannot rely uniquely on experimental activities. Nowadays, zero-dimensional/one-dimensional (0D/1D) numerical codes can be exploited during the early engine development phase in order to reduce the effort of testing campaigns and to speed up the development process of new engines. By relying on predictive phenomenological combustion models, fast and accurate predictions of the engine performance can be obtained, thus driving the optimization of engine operating parameters and virtually assessing the potential of new technologies and engine modifications. Nevertheless, the proper simulation of the DF combustion process remains a challenging task to be addressed within a 0D/1D simulation framework due to the complex combustion phenomenon which involves two fuels characterized by different burning properties.

In this regard, many researchers recently worked on the development of DF combustion models, exploring both numerical and phenomenological simulation approaches. A multi-Wiebe combustion modeling approach was exploited both by Xu et al. [16] and Barro et al. [17] to describe the DF combustion as a superposition of spray and premixed-charge combustion processes. Nandagopal et al. [18] presented a data-driven modeling approach to simulate the heat release rate (HRR) in DF engines operating with renewable fuels. In the framework of fully phenomenological models, Zirngibl et al. [19] developed and validated a DF model which combines a quasi-dimensional packets modeling of the pilot injection process with phenomenological modeling of the spreading hemispherical and turbulent flame front of the main combustion. A similar approach was proposed also by Taritas et al. [20]. Differently from [19], in that work the oxidation of the primary fuel is simulated by means of a multi-flames model, taking into account the multiple flame kernels generated by the different spray plumes combustion. Focusing on large-bore engines applications, Krenn et al. [21] proposed a phenomenological model for the DF combustion simulation based also in this case on a two-stage modeling approach to handle the pilot fuel combustion and the subsequent flame propagation.

In line with other works in the literature, in this article a predictive combustion model for DF engines is presented. The model describes the pilot fuel injection by means of a multi-packets Lagrangian approach, and the subsequent phases of the fuel breakup, evaporation, entrainment of the premixed air-gas mixture inside the diesel jet, and, finally, its combustion. The diesel fuel autoignition triggers the flame propagation of the premixed air-gas mixture, which is simulated by means of entrainment and burn-up approach. The overall combustion process is therefore modeled as a superposition of the combustion in the spray and the air-gas mixture oxidation by a propagating spherical turbulent flame. The two combustion modes are coupled via a transition function, based on the physical characteristics of the spray and the flame. Several sub-models, namely, ignition delay,

laminar, and turbulence flame speed models, were specifically optimized for the operating conditions of large-bore pilot-ignited DF engines. In addition to this, with the aim to extend the validity of the model also in terms of emission predictions, a NOx emissions model was developed. The NOx model, which is based on the well-known Zeldovich mechanism, accounts for the mixture composition and temperature distribution of the burned gasses in the cylinder by dividing the overall cylinder volume into multiple zones and separately computing their temperature evolution and related NOx formation. The proposed combustion model was validated on a comprehensive dataset of experimental data from a Wärtsilä laboratory Single-Cylinder Engine (SCE), which includes variations of the main hardware (Compression Ratio [CR], valve timings) and calibration parameters (pilot fuel specifications, boost conditions) at different engine loads.

The article is structured as follows: after a brief introduction of the case study, a detailed description of the developed DF combustion model is presented; finally, the predictive capabilities of the numerical model are evaluated both in terms of combustion-related results and NOx emissions predictions.

2. Case Study

The case study selected for the development and the validation of the DF combustion model is the Wärtsilä 31DF SCE, whose main technical data are shown in Table 1.

This engine family achieves a very low fuel consumption level, complying at the same time with IMO Tier III NOx regulations, by exploiting state-of-the-art technologies for the air control (two-stage turbocharger and variable valve actuation) and fuel injection (highly flexible common rail injection system).

An extensive experimental campaign was conducted on the Wärtsilä 31DF SCE, with the aim to investigate the DF combustion process and the influence of several engine parameters, such as pilot injection strategy (i.e., rail pressure, injection timing, and duration), boost conditions, valve timings, and CR. The wide experimental dataset, which features more than 100 different engine conditions allowed to perform a comprehensive validation of the developed DF combustion model.

TABLE 1 Wärtsilä 31DF engine technical data (data taken from Ref. [22]).

Specification	Unit	Value
Cylinder bore	mm	310
Piston stroke	mm	430
Cylinder rated power	kW/cyl	550
Engine speed	RPM	750
BMEP	bar	27.2

3. DF Combustion Model

In the cylinder, a multi-zone phenomenological model is used, which tracks various stages of the combustion process. Initially, all mass in the cylinder is contained in a single thermodynamic zone, the *main unburned zone*. The air and gas flow from intake valves get added to the main unburned zone. Once the pilot diesel fuel is injected, a new zone in the cylinder is introduced—the *spray zone*. The diesel fuel from the injector is progressively added to this zone according to a defined injection rate, required as an input for the developed model. All zones can exchange mass and energy with each other, and the thermodynamic state of the zones is updated every timestep.

As the spray propagates into the cylinder, it entrains the surrounding air-gas mixture. After a period of physical (evaporation, mixing) and chemical ignition delay, combustion is initiated in the spray. At this time, a third thermodynamic zone is introduced in the cylinder—the *burned zone*. As combustion progresses in the cylinder, mass and energy are transferred from the main unburned and spray zones to the burned zones at a rate governed by the combustion models employed.

The combustion process in the cylinder is modeled as a superposition of two modes of burning—combustion in the spray by a "jet-flame" and combustion in the air-gas mixture by a propagating spherical turbulent flame brush. A transition function, based on the physical characteristics of the spray and the flame, is used to smoothly shift from one mode of burning to the other. A pictorial representation of this process is shown in Figure 1.

3.1. Spray Combustion Model

This section describes the sub-model which is used to track the evolution of processes inside the spray. A Lagrangian approach, similar to the one presented in [22], is adopted to model the spray. As the spray enters the cylinder, it is discretized into parcels along the spray axis, and the evolution of these parcels is tracked in time. Spray discretization in the radial direction is not performed in the interest of maintaining model simplicity and speed of computation. Each parcel can continuously mix with the surrounding gases (in the main unburned and burned zones) and with other parcels that exist in the cylinder. In tracking the evolution of these parcels, the following processes are modeled—penetration of the parcel into the cylinder, evaporation of the liquid fuel, entrainment of gas into the parcel, chemical ignition delay, and, finally, combustion.

3.1.1. Penetration, Evaporation, and Entrainment

Two quantities govern the evolution of spray parcels inside the cylinder, namely, penetration distance and velocity. In the current study, a modified version of the correlations developed by Jung and Assanis [23] were primarily adopted, which are based on the model proposed by Hiroyasu and improved to handle nozzles with arbitrary discharge coefficients and to obtain a better match to the experimental measurements.

FIGURE 1 Schematic representation of DF combustion modeling.

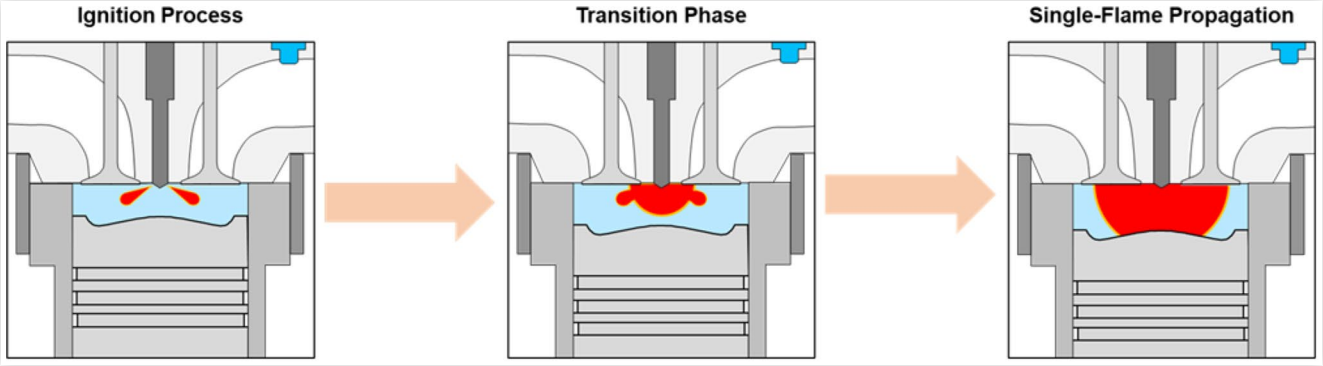

However, recent studies highlighted the limitations of the Hiroyasu model in describing the spray penetration in the case of short injection events, and the need to track the parcel evolution in a specific way after the end of the injection (EOI). More in detail, after the EOI, studies have shown that the spray undergoes significant deceleration with increased rates of entrainment. Musculus et al. [24] have studied this phenomenon using a 1D discrete model for diesel jets. Immediately after EOI entrainment rates were enhanced by a factor of two to three near the tip of the injector. This increased entrainment then moves downstream toward the tip of the spray after EOI, which is what was termed as the *entrainment wave*. Such increased entrainment rates can alter the composition inside the spray and, in turn, impact the ignition delay timing, particularly in diesel pilots with small injection durations and early timings. In the current study, parcels penetration and velocity correlations were further modified to account for these effects after EOI. The modifications have been carried out based on the correlations developed in Zhou et al. [25]. In the proposed correlations, the dependence of spray penetration distance on time changes from a $\sim t^{0.5}$ scaling to a $\sim t^{0.25}$ scaling during the decelerating stage of the spray after EOI. The final parcel correlations used in the current study are reported in Equation 1.

$$S = \begin{cases} u_{inj} t \, f_1\left(\dfrac{t}{t_b}\right) & t \le t_b \\ u_{inj} t^{0.5} \, f_2\left(\dfrac{t}{t_b}\right) & t_b \le t < 2t_i \\ u_{inj} t_i^{0.25} \left(t - t_i\right)^{0.25} f_3\left(t_b\right) & t \ge 2t_i \end{cases} \qquad \text{Eq. (1)}$$

$$u = \frac{dS}{dt}$$

where S is the penetration distance of the parcel; u is the instantaneous parcel velocity; t is the time elapsed since the creation of the parcel; u_{inj} is the velocity of the spray at the injector nozzle, estimated using the mass flow rate profile given as an input to the model, the fuel density and injector nozzle geometry; t_i is the time elapsed between the creation of the parcel and the related EOI pulse the parcel belongs to; and t_b is the breakup time, which is defined as the time up to which the jet travels as a liquid column and beyond which it atomizes into droplets evaluated according to Equation 2.

$$t_b = 4.351 \sqrt{\frac{2\rho_l}{\rho_g}} \frac{d_n}{C_d u_{inj}} \qquad \text{Eq. (2)}$$

where ρ_l is the density of the injected liquid, ρ_g is the density of the surrounding gas, d_n is the nozzle hole diameter, and C_d is the discharge coefficient of the injector nozzle.

As the spray parcel travels inside the cylinder, it continuously entrains mass and slows down. The rate of entrainment of gases inside a parcel is modeled by assuming conservation of the initial parcel momentum, as reported in Equation 3.

$$\frac{dm_{es}}{dt} = -C_e \frac{m_{inj} u_{inj}}{u^2} \frac{du}{dt} \qquad \text{Eq. (3)}$$

where m_{inj} is the initial mass of the parcel, m_{es} is the mass entrained in the spray parcel, and C_e is a calibration parameter, which compensates for effects that this simple spray model does not capture.

The model used for the evaporation of liquid fuel inside a parcel is based on the work by Wahiduzzaman et al. [22]. It is assumed that the fuel in each parcel breaks up into small droplets. The Sauter Mean Diameter (SMD) of the droplets (d_d) is calculated based on the expression given in Equation 4.

$$\frac{d_d}{d_{noz}} = 60 \, Re^{-0.22} We^{-0.31} \left(\frac{\rho_l}{\rho_g}\right)^{-0.17} \qquad \text{Eq. (4)}$$

where *Re* is the Reynolds number, *We* is the Weber number, and d_{noz} is the injector nozzle diameter. The evolution of the mass of a droplet due to evaporation is given by Equation 5.

$$\frac{dm_d}{dt} = -\pi d_d \rho_g \alpha_g Shlog\left(1 + B_m\right) \qquad \text{Eq. (5)}$$

where α_g is the diffusivity of the gas, *Sh* is the Sherwood number, and B_m is the Spalding mass transfer number. The change in droplet temperature (T_d) due to convective heat transfer and evaporative cooling is given by Equation 6.

$$\frac{dT_d}{dt} = \frac{1}{m_d c_{p,d}}\left(\frac{dQ_d}{dt} - \frac{dm_d}{dt}\Delta H_{v,d}\right) \qquad \text{Eq. (6)}$$

where $c_{p,d}$ is the droplet heat capacity, Q_d is the convective heat transfer from the gas to the droplet, and $\Delta H_{v,d}$ is the droplet enthalpy of evaporation. The coupled heat and mass transfer solution appropriately accounts for both diffusion-limited and boiling-limited evaporation.

3.1.2. Ignition Delay As far as the ignition delay is concerned, the well-known Livengood-Wu approach [26] is employed for evaluating the ignition delay period, i.e.,

$$\int_{t_{inj}}^{t_{ign}} \frac{1}{\tau} dt = 1 \qquad \text{Eq. (7)}$$

where the term τ represents the ignition delay for a homogeneous mixture characterized by constant physical properties at a given timestep. The term τ is computed according to a specific formulation for large-bore DF engines developed in a previous work by the authors [27]. The model was developed and correlated considering 0D-Computational Fluid Dynamics (CFD) calculations performed with the Ranzi et al. [28] chemical kinetics mechanism (130 species and 2323 reactions), selecting the *n*-dodecane as surrogate for the pilot diesel fuel. The simulation test matrix considered pressure, temperature, air-to-diesel equivalence ratio, and CH_4 content variations within specified ranges representative of the typical DF engine operations. The calculations showed the need to take into account the inhibitory contribution of CH_4, which chemically reacts with oxygen, hindering the oxidation process of diesel in particular under low temperature and very diluted diesel conditions, as confirmed in the literature both by numerical and experimental works [29, 30, 31]. The accuracy of the proposed ignition delay model can be evaluated from Figure 2, in which the predicted ignition delay values are depicted against the results of the detailed chemistry 0D-CFD calculations, considering variations in terms of pressure, temperature, and mixture conditions typical of a pilot-ignited DF engine operation. In detail, the pressure was varied from 40 bar to 100 bar, temperature from 650 K to 800 K, diesel-air equivalence ratio from 0.4 to 1.4, and CH_4 concentration in the 2-3% range.

Compared to the reference formulation presented and extensively commented in [27], the ignition delay model was

FIGURE 2 Ignition delay correlation plot.

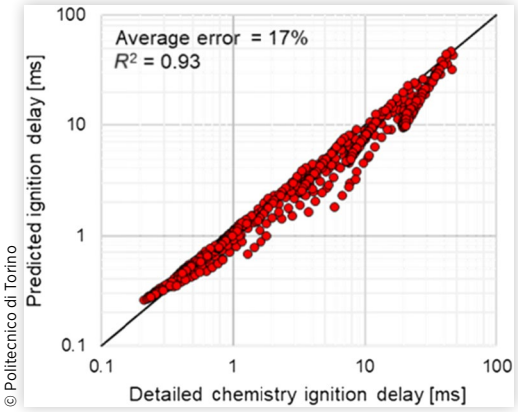

subsequently refined, aiming to take into account the Cetane Number (CN) of the fuel. As a matter of fact, in terms of chemical kinetics, the composition of the mixture of hydrocarbons composing the diesel fuel influences the energy threshold required to activate the oxidation reactions. This parameter is accounted for in Arrhenius-like equations by the coefficient in the exponential term, in many cases referred to as the apparent activation energy. The CN, which should remain within a certain range for the DF operation, shows a dependence on the apparent activation energy of the fuel [32]. Indeed, to consider the fuel CN, the ignition delay model was improved in the herein study and the updated formulation is reported in Equation 8.

$$\tau = C_{ign} \exp\left(\frac{f(CN)}{T}\right) p^{-0.27} x_{O_2}^{2.8} \left(1 + 2.8 \cdot 10^{-2} \frac{x_{CH4}}{x_{diesel}^{2.12}}\right) \qquad \text{Eq. (8)}$$

where T and p are the temperature and the pressure in the spray zone region, respectively, while x_{O_2}, x_{diesel}, and x_{CH_4} represent the mass concentrations of oxygen, diesel fuel, and CH_4, respectively. C_{ign} represents a tuning parameter, which can be optimized during the DF combustion model correlation.

The cetane number function $f(CN)$, given in Equation 9, is based on the work of Hardenberg [32], in which a hyperbolic dependence between apparent activation energy and CN was highlighted.

$$f\left(CN\right) = \frac{k_1}{CN + k_2} \qquad \text{Eq. (9)}$$

The coefficients k_1 and k_2 reported in Equation 9 were optimized directly against engine data from the considered case study. The minimization of error between the experimental and the predicted ignition delay (defined as the interval from Start of Injection (SOI) to 2% of Burned Fuel Fraction (MFB-2)) was carried out by considering a load variation performed with a CN-54 and CN-40 pilot fuel. The results of the ignition delay model for the two different CN levels are presented in Figure 3, in which a comparison between

FIGURE 3 Comparison between experimental and predicted ignition delay results for a load variation considering a CN = 54 and CN = 40.

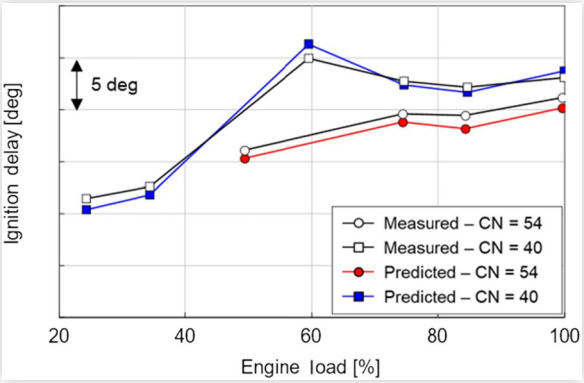

experimental and predicted data in terms of ignition delay is depicted. Since the two datasets were performed with the same engine calibration, the effect of the CN variation can be pointed out from the plot: moving from CN-54 to CN-40, the ignition delay increases by approximately 5 degrees (deg) in the considered DF engine operation. The ignition delay model is able to replicate correctly the experimental results by properly capturing the sensitivity of the CN on the ignition delay and reaching an absolute error lower than 1.5 deg for the two considered load variations.

3.1.3. Combustion Inside the Spray Combustion in the spray is modeled in two stages: premixed burning and diffusion burning. At ignition the evaporated fuel and entrained gas mass within a parcel are set aside as *premixed mass* (m_{pre}), and the burning of this mass is modeled assuming a rate representative of a propagating flame. The premixed burn rate formulation is given in Equation 10.

$$\frac{dm_{pre}}{dt} = C_{pm} m_{pre} \left\{ u_{pre} \left(t - t_{ign} \right) \right\}^2 f_{pre} \left(\phi, EGR \right) \qquad \text{Eq. (10)}$$

where C_{pm} is a calibration parameter, t_{ign} is the time ignition was initiated in the parcel, and f_{pre} is a function accounting for the slowdown of combustion due to lack of oxygen in the cylinder, either due to high levels of dilution or close to stoichiometric mixtures. Similar formulations of premixed burning, with a quadratic dependence on time elapsed since ignition, have been used by other works in literature [33, 34].

After ignition, the spray parcels continue to entrain the air-gas mixture. The gas mixture within the parcels, the mass of which is denoted by m_{diff}, is now burned with a diffusion-limited or mixing-controlled rate, given by Equation 11.

$$\frac{dm_{diff}}{dt} = C_{diff} m_{diff} \frac{\sqrt{k}}{\sqrt[3]{V_{cyl}}} f_{diff} \left(y_{O_2} \right) \qquad \text{Eq. (11)}$$

where C_{diff} is a calibration parameter, k is the turbulence intensity in the cylinder, V_{cyl} is the instantaneous cylinder volume, and f_{diff} captures the reduction in burn rate to the reduced oxygen concentration (i.e., increased residuals). The formulation of the diffusion rate adopted here is similar to the one presented by [35].

The total burning rate inside the spray can now be expressed according to Equation 12.

$$\frac{dm_{bs}}{dt} = \frac{dm_{pre}}{dt} + \frac{dm_{diff}}{dt} + \dot{s}_f m_{us}$$

$$\dot{s}_f = \frac{1}{m_u} \frac{dm_{bf}}{dt} \qquad \text{Eq. (12)}$$

$$\frac{dm_{us}}{dt} = \frac{dm_{es}}{dt} - \frac{dm_{bs}}{dt}$$

where m_{bs} is the mass added to the burned zone from the spray unburned zone, m_{bf} is the mass added to the burned zone from the flame, m_u is the total unburned mass in the cylinder, and m_{us} is the mass of the spray unburned zone. The last term in the spray burning rate equation, $\dot{s}_f m_{us}$, is a source term that couples combustion in the spray with combustion occurring behind the flame brush. The rationale behind including such a source term will be provided below.

3.2. Turbulent Propagating Flame Model

Burning by the turbulent flame brush is modeled by the propagation of a single spherical flame governed by an entrainment and burn-up model [36]. Propagation of the flame is started from a fixed location inside the cylinder (currently defined as the injector tip location). As the flame brush propagates, it entrains mass, which is then burned behind the flame over a characteristic timescale. The equations governing the model are reported in Equation 13.

$$\frac{dm_{uf}}{dt} = \rho_u A_e S_T - \frac{dm_{bf}}{dt}$$

$$\frac{dm_{bf}}{dt} = \frac{m_{uf}}{\tau} + \dot{s}_s m_{bf} \qquad \text{Eq. (13)}$$

$$\tau = \frac{C_l \lambda}{S_L}; \quad \dot{s}_s = \frac{1}{m_b} \frac{dm_{bs}}{dt}$$

where m_{uf} and m_{bf} are unburned mass entrained by the flame brush and the burned mass behind the flame brush, respectively; m_b is the total burned mass in the cylinder; ρ_u is the density of the unburned mixture; A_e is the entrainment surface area of the flame; S_T and S_L are the turbulent and laminar flame speeds, respectively; τ is the characteristic burning timescale, and $\dot{s}_s$ is a source term coupling the combustion behind the flame to the combustion in the spray. The correlations used to calculate the laminar and turbulent

flame speeds will be discussed in the forthcoming sections. The turbulent flame speed S_T and the burning timescale τ are functions of turbulence quantities, namely, the intensity u' and Taylor microscale $\lambda = l/Re_T$, calculated using the integral length scale l and turbulent Reynolds number Re_T. All turbulence-related quantities (l and u') are provided by the $K-k-\epsilon$ turbulence sub-model used in the cylinder [37].

As it can be argued from the formulations considered to describe the flame propagation, a proper evaluation of both laminar velocity and turbulence velocity are therefore of fundamental importance to correctly describe the oxidation process of the primary fuel. For this reason, in this work a detailed analysis on both laminar and turbulent flame speed models was carried out, with the aim of improving the accuracy of the combustion model in the case of DF engine operating conditions.

3.2.1. Laminar Flame Speed Starting from the laminar flame speed, an empirical correlation is exploited within the simulation platform based on the well-known power-law formulation reported in Equation 14, widely adopted in literature, and firstly introduced by Metghalchi and Keck [38].

$$S_L = (\phi, T_u, p_u) = S_{L0}\left(\frac{T_u}{T_0}\right)^{\alpha}\left(\frac{p_u}{p_0}\right)^{\beta} f(dilution) \qquad \text{Eq. (14)}$$

where S_{L0} is the velocity at $T_u = T_0 = 298$ K and $p_u = p_0 = 1$ atm for a given equivalence ratio ϕ, and it is computed for the CH_4 fuel according to the Gülder formulation [39]; α and β, exponents of temperature and pressure terms, respectively, are function of the equivalence ratio. The latter term $f(dilution)$, not present in the original expression, is considered to account for the effect of burned species (CO_2, H_2O) in the flame, deriving from residuals or externally recirculated exhaust gasses, and it is reported in Equation 15.

$$f(dilution) = 1 - 0.75\, C_{dil}\left(1 - \left(1 - 0.75\, C_{dil}\, y_b\right)^7\right) \qquad \text{Eq. (15)}$$

where y_b represents the burned gasses mass fraction and C_{dil} is a tuning parameter, which can be optimized during the combustion model calibration.

According to the reference formulation for CH_4 fuel, which is based on the work of Amirante et al. [40], α and β are expressed as second-order polynomial function over the equivalence ratio, as reported in Equation 16.

$$\alpha = a_2\,\phi^2 + a_1\phi + a_0$$
$$\beta = b_2\,\phi^2 + b_1\phi + b_0 \qquad \text{Eq. (16)}$$

However, at high-pressure conditions (>150 bar) the reference model showed unrealistic low laminar flame speed, thus requiring a revision and an additional optimization of the model. For this objective, in line with other research studies [41, 42], the laminar flame speed was investigated by means of 1D-CFD calculations, carried out considering four different reaction mechanisms. Among the selected four kinetic schemes, presented in Table 2, the GRI 3.0 and USC Mech II describe the chemical kinetics for fuels with low carbon content, while both Ranzi and Narayanaswamy are optimized to include the oxidation of alkanes up to *n*-dodecane. The laminar flame calculations were performed in the engine-relevant thermodynamics and mixture conditions, namely, 40-180 bar as pressure range, 700-1000 K as temperature range, and equivalence ratio level ranging from 0.35 to 0.55. The results of the laminar flame speed calculations are reported in Figure 4. A sweep of the equivalence ratio at 100 bar and 800 K is proposed in Figure 4(a), while a pressure sweep from 60 bar to 180 bar is reported in Figure 4(b) at constant temperature (800 K) and equivalence ratio (0.5). Among the four kinetic schemes considered for this analysis, the GRI 3.0 kinetic scheme showed the largest values of laminar flame speed in all the considered conditions, while the other three reaction mechanisms produced very similar results.

TABLE 2 Reaction mechanisms considered for the laminar flame speed model correlation.

Mechanism name	Fuel	Species	Reactions	Reference
GRI 3.0	CH_4	53	325	[43]
USC Mech II	C_1-C_4	111	784	[44]
Ranzi	C_{12}	130	2323	[28]
Narayanaswamy	C_{12}	255	1512	[45]

FIGURE 4 Laminar flame speed model results compared to the 1D-CFD calculations: (a) equivalence ratio sweep at 100 bar and 800 K; (b) pressure sweep at PHI = 0.5 and 800 K.

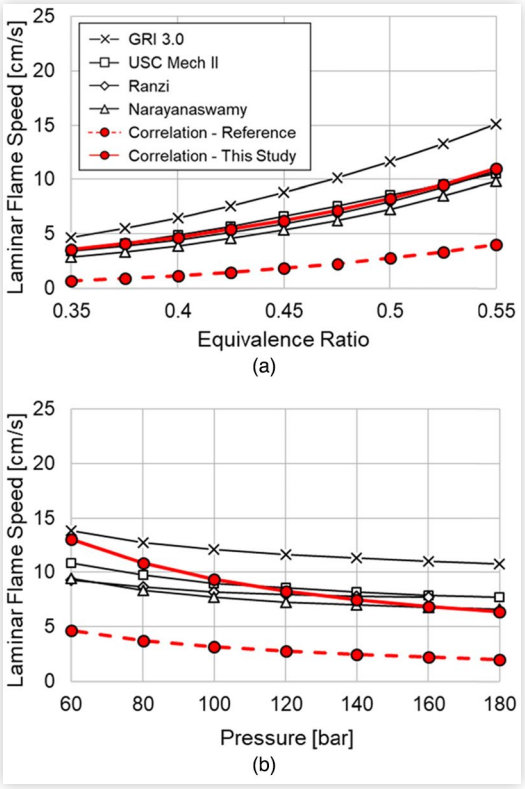

TABLE 3 Reference and optimized coefficients for exponents α and β.

	a_2	a_1	a_0	b_2	b_1	b_0
Reference	4.9199	–10.287	6.9258	–1.3712	2.6808	–1.7492
This study	–14.078	14.125	0.1172	4.0863	–4.3993	0.5229

The obtained laminar flame speed values were therefore used for the refinement of the laminar flame speed model. Since the S_{L0} term, expressed by the Gülder formulation, showed satisfactory results with respect to the selected reaction mechanisms, only the coefficients involved in α and β functions were considered in the optimization process.

The reference and the optimized coefficients proposed for the exponents α and β are reported in Table 3.

Looking at the results given in Figure 4, the results of the reference laminar flame speed model evidence a significant underestimation of the laminar flame speed, which would result in a very slow combustion process if the reference correlation would be considered within the DF combustion model. On the contrary, the optimized laminar flame speed model provides results in a very good agreement with the outcomes of the considered kinetic schemes.

Eventually, the kinetic schemes optimized for *n*-dodecane oxidation, whose results are aligned to the USC Mech II mechanism, were further exploited for the evaluation of the contribution of a small amount of diesel vapor on the laminar velocity of an air-gas mixture. In fact, from experiments on the herein case study and also on similar test cases [46], a fast combustion process can be observed when the ignition delay period is significantly prolonged (>20 deg). This behavior could be linked to the fact that the injected diesel fuel almost totally mixes in the cylinder, and it can contribute to speed up the early stage of the flame propagation. In this regard, preliminary laminar flame speed calculations were conducted at 800 K over a pressure sweep considering a $\phi = 0.5$ CH_4-air mixture as a reference, and the impact of a 0.5% of dodecane added to the original composition (which leads to a PHI level very close to 0.58) was investigated. The results reported in Figure 5 confirmed that an addition of 0.5% of dodecane in the reference CH_4-air mixture leads to an almost doubled laminar flame speed. This increment is not only due to the higher energy density characterizing the DF mixture but also due to the different reactivity of the two fuels. In fact, if the green curve, which depicts the DF case, is compared to the blue curve, which represents a CH_4-air mixture with the same equivalence ratio, a significant enhancement of the laminar flame speed can be noted, in this case only due to the different chemical properties of the two mixtures. To address the need to consider both the CH_4 and the overmixed pilot fuel in the laminar flame speed evaluation, a methodology was proposed by Eder et al. [47] for a 3D-CFD simulation study, which is based on the interpolation between tabulated *n*-heptane and CH_4 laminar flame speed values according to the related mass fraction in the flame. To consider the contribution of high-reactive diesel fuel on the flame velocity, a detailed 3D-CFD simulation analysis should be carried out in order to evaluate both the amount and the penetration of the fuel not burned during the initial ignition process and subsequently involved in the CH_4-air flame combustion, which reasonably depends on the engine operating condition. In this work this phenomenon was not considered, but it represents one of the main future developments for improving the accuracy of the DF model.

FIGURE 5 Laminar flame speed calculations for *n*-dodecane-CH_4-air mixture.

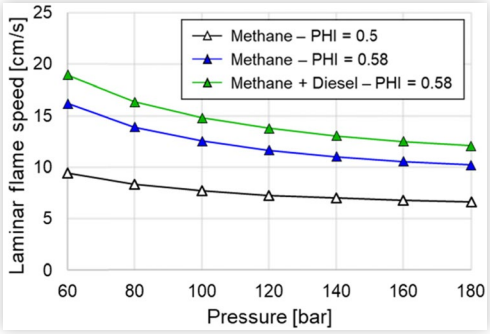

3.2.2. Turbulent Flame Speed

Moving to the turbulent flame speed (S_T) evaluation, the comprehensive work of Burke et al. [48] was considered as a starting point for the selection of the most appropriate correlation for the lean-burn DF case among those already available in literature. Although several studies have been conducted by researchers, there is not a unique formulation for determining S_T, due to the complex nature of turbulent flames. In the abovementioned study, among several models available in literature, the Muppala correlation [49] emerged as the model showing the lowest average deviation from experimental measurements considering different turbulence regimes. Interesting results were achieved with the correlation proposed by Kobayashi [50] as well, with an overall error larger than the Muppala correlation, but qualitatively capturing the main trends among the different turbulent regimes. Both correlations include an explicit pressure term, while models without neither an implicit nor explicit pressure dependence provided worse results. Similar considerations were addressed by Ratzke et al. in [51], in which the turbulence flame speed was indirectly evaluated from the experimental cylinder pressure, 3D-CFD analysis, and laminar flame speed calculations for a research single-cylinder gas engine, covering different dilution levels and engine speeds and maximum pressure up to 7 MPa. Also, in this case, the best agreement was obtained with correlations involving a pressure-depen-

TABLE 4 Turbulent flame speed correlation investigated in this study.

Name	Correlation	Ref.
Reference	$\frac{S_T}{S_L} = 1 + C_{TFS}\frac{u'}{S_L}$	[52]
Kobayashi	$\frac{S_T}{S_L} = C_{TFS}\,2.9\left(\frac{u'}{S_L}\right)^{0.38}\left(\frac{p}{0.1\text{MPa}}\right)^{0.38}$	[50]
Muppala	$\frac{S_T}{S_L} = 1 + C_{TFS}\frac{0.46}{Le}Re_T^{0.25}\left(\frac{u'}{S_L}\right)^{0.3}\left(\frac{p}{0.1\text{MPa}}\right)^{0.2}$	[49]

dency, either explicitly with an own pressure-term or implicitly from the pressure dependency of the turbulent Reynolds number. Moreover, the Kobayashi formulation showed a very good agreement with the calculated S_T values in lean conditions ($\phi < 0.6$), while Muppala correlation provided lower deviation for richer mixtures. In view of the above-mentioned relevant literature studies on CH_4 turbulent flame speed modeling, in this activity, the three correlations reported in Table 4 were considered for the DF combustion model. Both Kobayashi and Muppala correlations were investigated and compared to a reference turbulence flame speed correlation [52] extensively adopted for conventional gasoline combustion simulation and originally proposed even in the DF combustion case. The turbulent flame speed correlations are based on laminar flame velocity (S_L), on turbulent flow properties (turbulence intensity u' and integral length scale L_T), and, in the case of Muppala correlation, on dimensionless numbers (turbulent Reynolds number Re_T, and Lewis number Le). A tuning parameter C_{TFS} is introduced in the GT-SUITE DF combustion model, which can be exploited to adjust the flame velocity, providing consequently a direct impact on the combustion duration.

More in detail, a comparison of the different correlations in terms of Burn Duration of 10-75 results over an engine load sweep is presented in Figure 6. For this analysis, the same set

FIGURE 6 Comparison between experimental and predicted burn duration of 10-75 over a load variation considering different turbulent flame speed models.

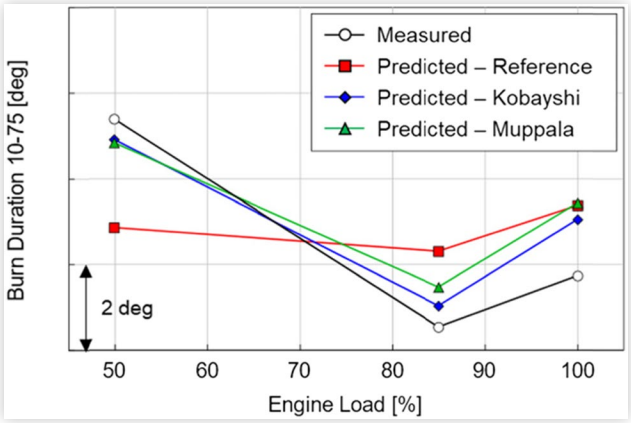

of tuning constants was adopted, with an exception for the C_{TFS} constant involved in the turbulent flame speed models, which were independently optimized according to the investigated formulation. The results show that Muppala and Kobayashi correlations provide very similar results in terms of flame speed and HRR, while the simplest reference formulation shows less accuracy in capturing the combustion duration over the considered load variation. The reference turbulent flame speed correlation leads to an almost constant predicted burn duration level, thus evidencing a limited sensitivity to the in-cylinder conditions. On the other hand, both Kobayashi and Muppala correlations allow to achieve a better agreement with experimental values, following the measured combustion duration with a maximum error lower than 2 deg.

Considering the limited difference between the two investigated correlations, and the lower complexity of the Kobayashi turbulent flame speed model, this latter was finally selected for the assessment of the predictive capabilities of the DF combustion model.

3.3. Coupled Operation of the Combustion Models

Since two modes of combustion are simultaneously active inside the cylinder, it is essential to ensure appropriate coupling between the two. After the mixture autoignition, the total unburned mass is composed of three parts: the unburned mass entrained by the spray, the unburned mass entrained by the flame brush, and the unburned mass which has not been entrained. When either the spray or the flame brush entrains mass, they are allowed to entrain from all the available unburned mass. The source term $\dot{s}_f$ in the jet burning equations (Equation 12) accounts for the fact that part of the unburned mass entrained by the jet can be entrained and burned by the flame brush, and similarly, the term $\dot{s}_s$ in the flame burning equations (Equation 13) accounts for the fact that part of the mass entrained by the flame brush can be entrained and burned by the jet.

As mentioned earlier, when combustion is occurring both in the spray and flame, a transition function is employed to gradually move from one combustion mode to the other. This transition function, similar to the one used by Walther et al. [53], is used to calculate the flame entrainment area A_e in the flame burning equation and is given in Equation 17.

$$A_e = \left(1 - \frac{R_f}{L_j}\right)A_{spray} + \left(\frac{R_f}{L_j}\right)A_{flame} \qquad \text{Eq. (17)}$$

where A_{spray} is the surface area of the spray, calculated by assuming the shape of the jet to be a truncated cone with a hemisphere at the bottom, A_{flame} is the surface area of the propagating spherical flame, R_f is the spherical flame radius, and L_j is the jet penetration. As combustion progresses in the cylinder, A_e is gradually transitioned from the surface area of the spray to the surface area of the propagating spherical flame.

4. NOx Modeling

In the current study, the formation and evolution of NOx in the cylinder is simulated using the well-established Zeldovich kinetic model [54]. It is well known that accurate NOx predictions require an accurate estimate of the temperature distribution inside the burned zone of the cylinder. In particular, burned gasses that are produced early in the combustion process continue to get compressed and reach temperatures higher than those attained immediately after combustion. This can have a significant impact on the levels of NOx produced. In order to capture this phenomenon, a stratified burned zone formulation was adopted for the evolution of the NOx kinetics. The burned zone in the cylinder is divided into 10 thermodynamic sub-zones. These sub-zones do not mix with each other, receive mass from the main and spray unburned zones, and can exchange heat with the cylinder walls. The combustion process, going from 0% to 100% fuel mass burned, is divided into 10 unequal subsections, with more focus toward the early phase of combustion, corresponding to the sub-zones. Mass from the spray and main unburned zones is added to the sub-zones during their respective section of the combustion process. As mass is being added to a particular sub-zone, the other sub-zones continuously get compressed and experience a rise in temperature. A pictorial representation of the multi-zone NOx emissions modeling is given in Figure 7.

Zeldovich NOx kinetics is evaluated in each sub-zone, using the temperature calculated in the sub-zone. The sum of NOx produced in each sub-zone is reported as the total NOx produced during combustion.

As an example, in Figure 8 the evolution of the temperature and related NOx formation in four different cylinder sub-zones are reported, referred to a 50% load operating condition and a lambda air-gas level of about 2.5. The first two zones—*Zones I and II*—account mainly for spray combustion and the initial phase of the flame propagation. *Zone I* considers the burned gasses from the spray combustion, whose temperature increases as the diesel fuel evaporates and ignites, and it is characterized by a final equivalence ratio level of 0.57. *Zone II* includes both the remaining part of the spray and the first part of fuel mass entrained and burned behind the flame

FIGURE 7 Schematic representation of multi-zone NOx emissions modeling.

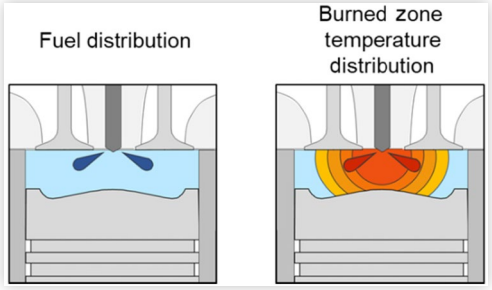

FIGURE 8 Temperature evolution and NOx formation on four simulated burned zones for a 50% load engine operating condition.

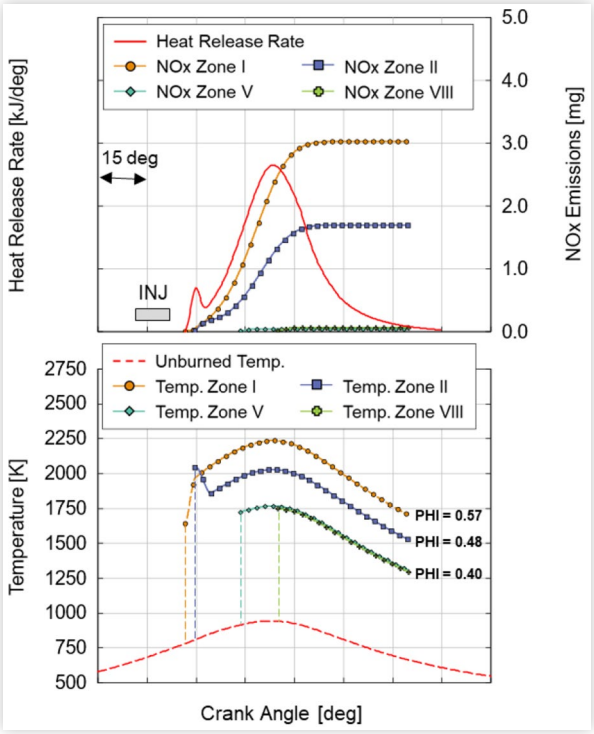

brush, thus showing an initial high-temperature level, which progressively reduces as the combustion evolves from spray to flame combustion. All the other zones—from *Zone III* to *Zone X*—include only burned air-gas mixture characterized by a lower equivalence ratio level (equal to 0.4), lower temperature, and, therefore, negligible NOx formation. The NOx emissions of each zone, depicted in the upper plot, are influenced by the temperature levels according to the Zeldovich mechanism and, for this operating condition, are mainly due to the combustion of the spray.

5. Results and Discussion

The developed DF combustion model was correlated with Wärtsilä 31DF SCE data. The tuning constants involved in the model, and summarized in Table 5, were optimized to minimize the deviation between the HRR predicted by the model and the HRR profiles obtained from the experimental pressure (average pressure of 300 consecutive engine cycle acquisitions). A reduced engine dataset, which includes 25 operating conditions randomly selected among the overall dataset, was defined for the calibration procedure. A single set of tuning parameters was optimized and kept constant for all the operating conditions. In line with a previous work on combustion model correlation [55], the Non-dominated Sorting Genetic Algorithm III (NSGA-III) algorithm was

TABLE 5 Tuning constants involved in the DF combustion model.

Pilot fuel autoignition tuning constants		
C_e	Spray entrainment rate constant	Equation 3
C_{ign}	Ignition delay constant	Equation 8
C_{pm}	Premixed combustion rate constant	Equation 10
C_{diff}	Diffusive combustion rate constant	Equation 11
Air/gas flame propagation tuning constants		
C_{dil}	Mixture dilution constant	Equation 13
C_{TFS}	Turbulent flame speed constant	Equation 13
C_l	Taylor length scale constant	Equation 15

exploited in GT-SUITE for the model optimization. Subsequently, the DF model, based on a single set of tuning constants, was validated on an extensive dataset, which includes 80 different operating conditions. The extensive dataset intended for the model validation allows to robustly assess the predictive capabilities of the proposed DF model over a wide range of engine conditions.

In this section the results of the predictive DF combustion model are presented, both in terms of in-cylinder pressure and HRR and in terms of main combustion parameters, compared to the experimental measurements.

Figure 9 shows the results of the predictive combustion model compared to the experimental results over four different variations, namely, engine load, SOI, lambda, and CR. In the figure, the injection event from the hydraulic SOI to the hydraulic EOI is depicted by the grey rectangular shapes. Starting from the load sweep, reported in the first row of Figure 9, the combustion process is faithfully reproduced by the model going from 50% to 100% engine load. The maximum firing pressure error is limited to 10 bar, and the phasing of the HRR is correctly captured. Focusing on the 50% load (Figure 9: first row, right), the effect of the higher temperature at the end of the compression stroke due to the reduced Miller level leads to a reduced ignition delay and pronounced combustion of the diesel spray if compared to the full-load case. The model is able to properly capture the effect of the temperature on the ignition timing, as well as to replicate the HRR during the early stage of the combustion. A similar behavior can be pointed out by analyzing the SOI sweep reported in the second row of Figure 9. If the SOI is advanced from the baseline calibration, the ignition delay is prolonged due to the lower temperature of the air-gas mixture, thus giving more time to the pilot diesel for mixing with air and leading to a lower local diesel concentration in the spray region. The combustion process of the leaner spray cloud is, therefore, less intense if compared to the baseline condition without showing a pronounced combustion of the spray. A limit condition instead is reported on the right picture, in which the SOI is retarded by 8 CA deg from the baseline level. In this case the pilot fuel ignites before the hydraulic EOI, as the higher temperature enhances the fuel evaporation and the kinetics of the diesel oxidation.

The developed predictive model is capable of providing an accurate simulation of the combustion process by capturing the effect of the SOI on ignition timing, spray combustion, and flame propagation. Accurate predictions were also obtained if a lambda variation is considered, as can be seen from the third row in Figure 9, thus confirming the accuracy of the laminar flame speed correlation optimized in this work. Moreover, if the bottom row of Figure 9 is considered, the accuracy level of the combustion model is preserved also if the CR is modified. The DF model is able to consider the variation of temperature and, consequently, ignition timing due to the different CR, as well as the effect of this engine feature on the combustion velocity.

The satisfactory agreement achieved by the developed combustion model is confirmed extending the validation to the whole experimental dataset as shown by the correlation plots in Figure 10. The dataset includes several engine settings variations, such as diesel injection specifications (rail pressure, injection duration, and injected quantity), valve timings (Miller levels and valves overlap), receiver conditions (boost pressure and temperature), CR, and variations of the engine load from 50% to 100% of the rated power, resulting in more than 100 different engine operating conditions. As it is possible to evaluate from Figure 10, the ignition delay error is limited to ±3 CA deg. The largest deviations with respect to the experimental data are obtained in the case of advanced injection strategies and larger Miller levels, thus observing very large ignition delay periods. These conditions could be considered out of the validity for the ignition delay model since the hypothesis of linearity for the fuel oxidation required by the Livengood-Wu approach could not be satisfied in these low-temperature conditions. As far as the Burn Duration 10-75 is concerned, a Root Mean Square (RMS) error of about 2.5 CA deg can be highlighted from the correlation plot. The combustion model well captures the effect of the lambda variation, while, on the other hand, it shows some limitation in capturing fast combustion evolutions which are typically related to engine conditions in which the ignition delay is significantly prolonged (>20 deg), and the subsequent combustion evolution was shown to be characterized by a very fast flame propagation.

In these conditions (i.e., very prolonged ignition delay period and large pilot fuel diffusion), the real combustion evolution is characterized by multiple distinct flames which are generated by the pilot fuel combustion, while the combustion process is modeled through a single hemispherical flame brush, which may lead to an underestimation of the flame area and, consequently, to the combustion velocity. In addition to this, in the case of a very long ignition delay, the momentum of the pilot fuel injected in the cylinder is completely dissipated into turbulent energy which enhances the spray entrainment, thus obtaining a very low level of diesel vapor concentration. Due to the large dilution of the diesel fuel, the related combustion process cannot be neatly separated in spray combustion and subsequent flame propagation, but a concurrent pilot autoignition and flame development is obtained, with this latter significantly enhanced by the presence of diesel vapor, thus leading to a speed-up of the combustion process. It is worth pointing out that these operating conditions,

FIGURE 9 Comparison between predicted (red lines) and experimental (black lines) in-cylinder pressure and HRR: (a) Load variation, (b) SOI variation, (c) Lambda variation, (d) CR variation.

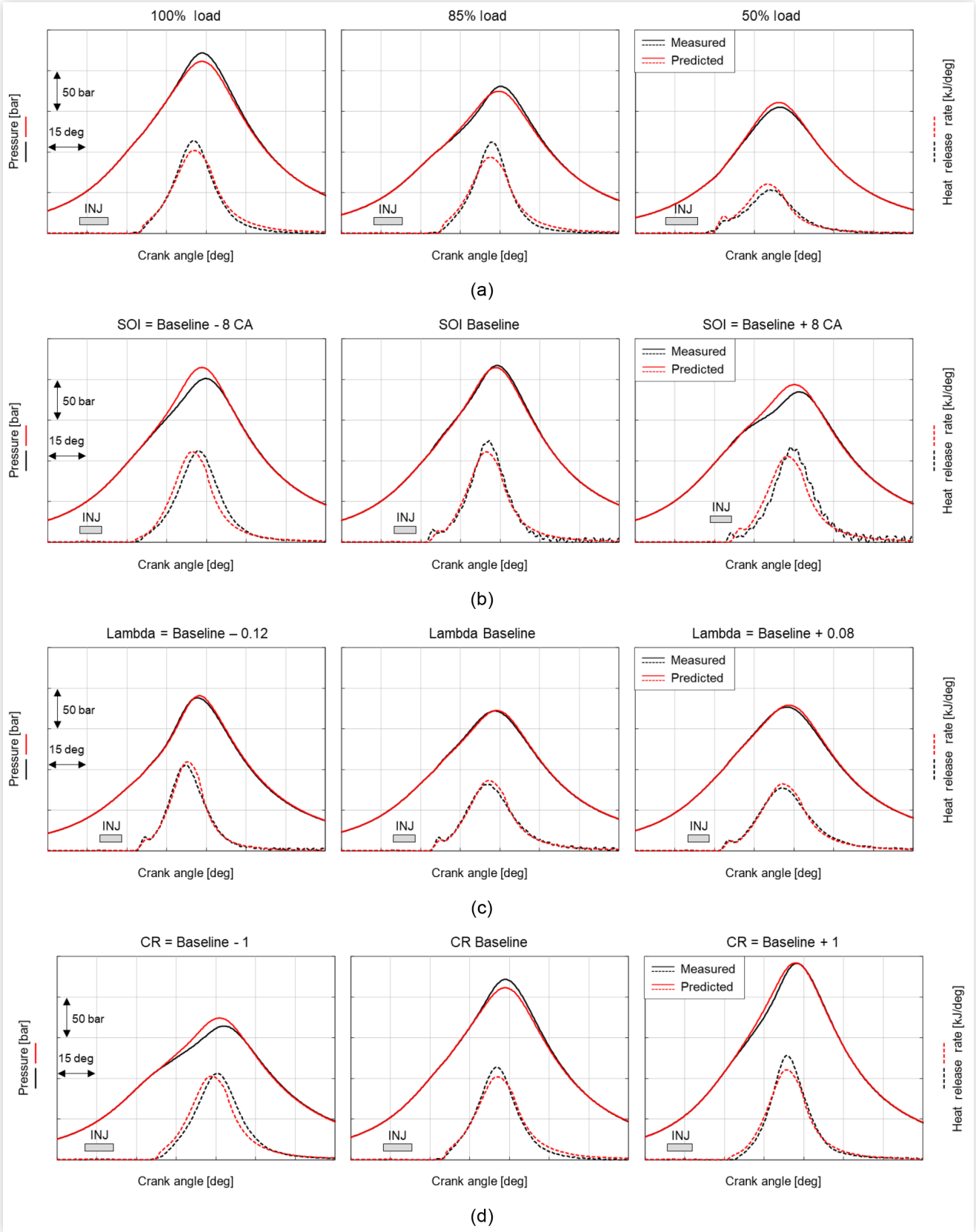

FIGURE 10 Correlation plot between measured and predicted results: ignition delay, combustion duration MFB1075, combustion anchor MFB50, maximum in-cylinder from left to right.

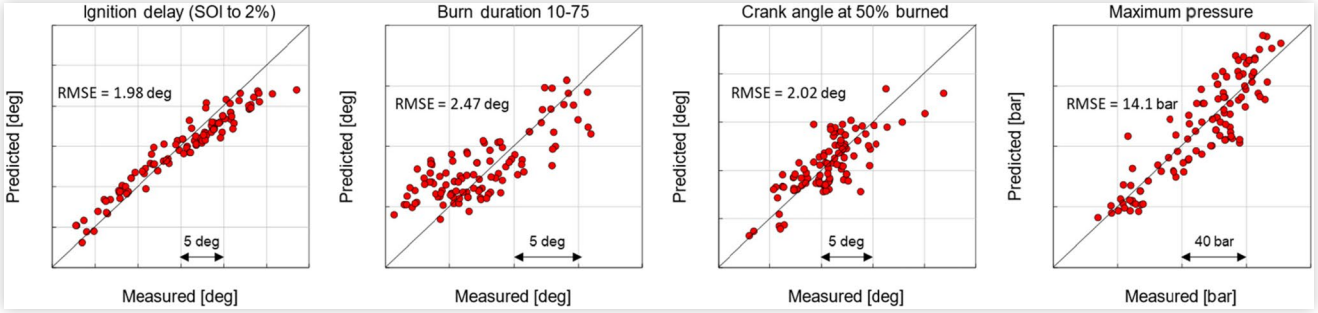

characterized by very early injections events and very small amounts of pilot fuel, represent limit conditions for the engine, and they are typically avoided during normal engine operation due to the large instability of the combustion process.

Although future developments of the combustion model are intended to increase the predictivity of the model also in these operating conditions, it is worth highlighting the satisfactory accuracy level reached by the model, which is able to provide reliable predictions of the main combustion parameters and capture the effect of the main engine calibration settings and hardware features on the combustion process. The resulting accuracy in terms of combustion anchor angle MFB-50, which is the result of both the ignition delay the combustion duration predictions, is characterized by an RMS error close to 2 CA deg, thus obtaining a satisfactory agreement in predicting the combustion phasing. The maximum in-cylinder pressure predictions are in good agreement with respect to the experimental measurements: an RMS error of 14 bar was obtained, and the maximum error is limited to about 30 bar. Both the MFB-50 and the maximum pressure RMS error are similar to the typical cycle-to-cycle variability ranges during engine operations, and therefore, the results predicted by the model would most likely lie within the range of variability of the real engine operation.

FIGURE 11 Results of NOx Zeldovich model compared to experimental results: (a) SOI variation at 50% load; (b) Lambda variation at high load operation.

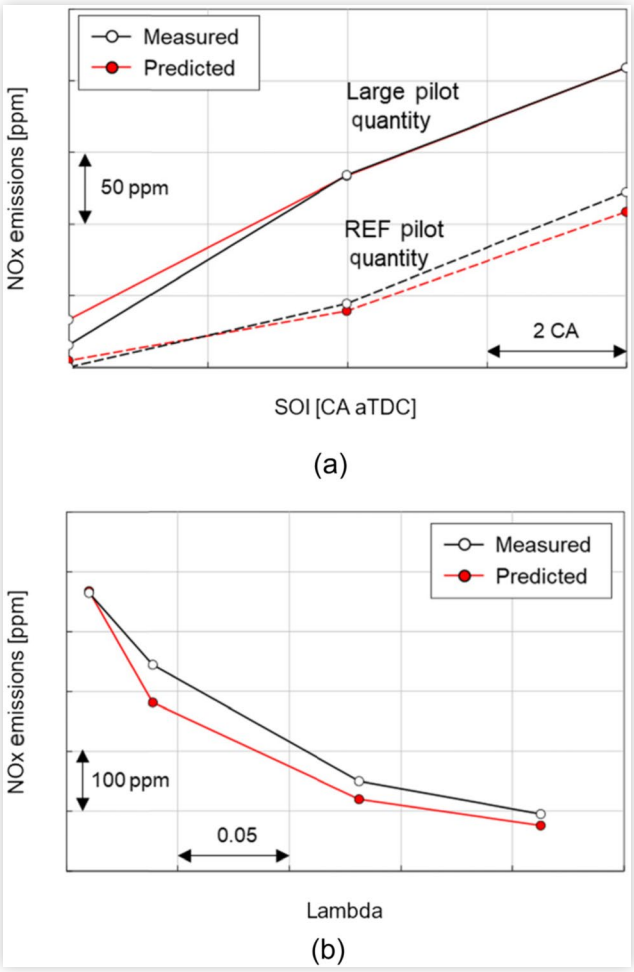

Moving to the NOx emissions prediction, a comparison between experimental and predicted results is reported in Figure 11 for an SOI variation at 50% load with different injected diesel quantity [Figure 11(a)] and over a lambda variation at high load engine conditions [Figure 11(b)]. As far as the SOI sweep is concerned, the lambda of the gas-air mixture was kept constant during the tests, and starting from a reference pilot fuel quantity (dashed line), the amount of injected fuel was increased by 50% (solid line) for a second SOI sweep. It is worth noting that the NOx emissions are significantly influenced by the injection strategy of the pilot fuel: as the pilot fuel is advanced, the NOx emissions reduce due to the higher spray dilution and, consequently, to the lower burned gasses temperature. In the case of a larger pilot fuel quantity, the energy density of the mixture in the spray region is larger, thus corresponding to enhanced NOx formation. The developed NOx emissions model, which considers the stratification of the charge and the different temperature levels in the burned gasses region, is able to provide very accurate predictions of the NOx emissions level and to properly capture the effect of the pilot fuel injection strategy with limited error for each tested condition. The high accuracy level of the NOx emissions model is confirmed even considering a lambda variation, reported in Figure 11(b), since the model is able to faithfully replicate the rise of the NOx emissions formation as the gas concentration in the premixed charge is increased.

6. Conclusions

In this article a novel multizone model for the simulation of the combustion process and NOx formation in large-bore Dual Fuel (DF) engines is presented. The developed DF combustion model considers a quasi-dimensional multi-packets modeling approach for the pilot fuel injection and the related spray formation while the subsequent homogeneous premixed gas oxidation is described by using a two-zone entrainment and burn-up approach. To properly account for the fuel properties in the combustion process, a previously developed ignition delay formulation was updated, considering not only the inhibitory effect of the CH_4 on the pilot fuel autoignition but also the reactivity of the pilot fuel by means of the fuel CN. On the other side, to properly reproduce the subsequent flame propagation, both laminar and turbulence flame speed models were improved with the aim to accurately mimic the entrainment and fuel oxidation in the flame at high pressure and, in the case of a lean mixture, typical operating conditions of large-bore DF engines.

A wide experimental campaign on a single-cylinder Wärtsilä research engine was carried out for the development and validation of the DF combustion model. To this aim, variations of engine load, pilot fuel injection strategy (i.e., injection timing, duration, and rail pressure), boost conditions, and engine features, such as CR and valve timings, were considered. The developed combustion model is capable to capture the influence of the abovementioned calibration parameters and engine hardware modifications on both combustion-related quantities and NOx emissions, providing accurate predictions in terms of ignition timing, combustion phasing, and peak cylinder pressure, thus paving the way for reliable virtual calibration activities.

Future developments of the model will be focused on the improvement of the predictive capabilities in very challenging conditions (e.g., extremely prolonged ignition delay period with advanced pilot SOI) by considering a multiple flame approach to simulate the DF combustion process.

Acknowledgment

Computational resources were provided by HPC@POLITO, a project of Academic Computing of the Politecnico di Torino (http://www.hpc.polito.it).

Moreover, the authors are thankful to AVL List GbmH for licensing AVL Concerto 5.4, used for experimental data post-processing, in the framework of the University Partnership Program.

Contact Information

Prof. Federico Millo
Politecnico di Torino | Energy Department (DENERG)
Corso Duca degli Abruzzi, 24 | 10129 Torino (ITALY)
federico.millo@polito.it
www.polito.it/engines

Abbreviations

BMEP - Brake Mean Effective Pressure
aTDC - after Top Dead Center
CA - Crank Angle
CFD - Computational Fluid Dynamics
CN - Cetane Number
DF - Dual Fuel
EEDI - Energy Efficiency Design Index
EOI - End of Injection
GHG - Greenhouse Gases
HRR - Heat Release Rate
IMO - International Maritime Organization
LHV - Lower Heating Value
LNG - Liquified Natural Gas
NOx - Nitrogen Oxides
NSGA-III - Non-dominated Sorting Genetic Algorithm III
SCE - Single-Cylinder Engine
SOC - Start Of Combustion
SOI - Start Of Injection
SMD - Sauter Mean Diameter

References

1. IMO, "Nitrogen Oxides (NOx)—Regulation 13," Air Pollut. GHG Emiss. 1, January 2013.
2. International Maritime Organization, "Sulphur Oxides (SOx) and Particulate Matter (PM)—Regulation 14, Air Pollut. GHG Emiss. 1, 2013.
3. Deng, J., Wang, X., Wei, Z., Wang, L. et al., "A Review of NOx and SOx Emission Reduction Technologies for Marine Diesel Engines and the Potential Evaluation of Liquefied Natural Gas Fuelled Vessels," *Sci. Total Environ.* 766 (2021): 144319, https://doi.org/10.1016/j.scitotenv.2020.144319.
4. Millo, F., Bernardi, M., and Delneri, D., "Computational Analysis of Internal and External EGR Strategies Combined with Miller Cycle Concept for a Two Stage Turbocharged Medium Speed Marine Diesel Engine," *SAE Int. J. Engines* 4, no. 1 (2011): 1319-1330, https://doi.org/10.4271/2011-01-1142.
5. Krishnamoorthi, M., Malayalamurthi, R., He, Z., and Kandasamy, S., "A Review on Low Temperature Combustion Engines: Performance, Combustion and Emission Characteristics," *Renew. Sustain. Energy Rev.* 116, no. September (2019): 109404, https://doi.org/10.1016/j.rser.2019.109404.
6. Schlatter, S., Schneider, B., Wright, Y.M., and Boulouchos, K., "Comparative Study of Ignition Systems for Lean Burn Gas Engines in an Optically Accessible Rapid Compression Expansion Machine," SAE Technical Paper 2013-24-0112, 2013, https://doi.org/10.4271/2013-24-0112.

7. Cho, H.M. and He, B.Q., "Spark Ignition Natural Gas Engines—A Review," *Energy Convers. Manag.* 48, no. 2 (2007): 608-618, https://doi.org/10.1016/j.enconman.2006.05.023.
8. Joung, T.-H., Kang, S.-G., Lee, J.-K., and Ahn, J., "The IMO Initial Strategy for Reducing Greenhouse Gas (GHG) Emissions, and Its Follow-Up Actions towards 2050," *J. Int. Marit. Safety, Environ. Aff. Shipp.* 4, no. 1 (2020): 1-7, https://doi.org/10.1080/25725084.2019.1707938.
9. Malfi, E., Bellis, V., Bozza, F., Cafari, A. et al., "A Phenomenological Model for the Description of Unburned Hydrocarbons Emission in Ultra-Lean Engines," *Int. J. Engine Res.* (2021), https://doi.org/10.1177/14680874211005063.
10. US EPA, "Understanding Global Warming Potentials—Greenhouse Gas (GHG) Emissions," 2020.
11. Sharafian, A., Blomerus, P., and Mérida, W., "Natural Gas as a Ship Fuel: Assessment of Greenhouse Gas and Air Pollutant Reduction Potential," *Energy Policy* 131 (2019): 332-346, https://doi.org/10.1016/j.enpol.2019.05.015.
12. Lindstad, E. and Rialland, A., "LNG and Cruise Ships, an Easy Way to Fulfil Regulations—versus the Need for Reducing GHG Emissions," *Sustainability* 12, no. 5 (2020): 1-15, https://doi.org/10.3390/su12052080.
13. Grochowina, M., Schiffner, M., Tartsch, S., and Sattelmayer, T., "Influence of Injection Parameters and Operating Conditions on Ignition and Combustion in Dual-Fuel Engines," *J. Eng. Gas Turbines Power* 140, no. 10 (2018): 1-10, https://doi.org/10.1115/1.4040089.
14. Singh, S., Krishnan, S.R., Srinivasan, K.K., Midkiff, K.C. et al., "Effect of Pilot Injection Timing, Pilot Quantity and Intake Charge Conditions on Performance and Emissions for an Advanced Low-Pilot-Ignited Natural Gas Engine," *Int. J. Engine Res.* 5, no. 4 (2004): 329-348, https://doi.org/10.1243/146808704323224231.
15. Weber, S., Stegmann, R., Prager, M., and Wachtmeister, G., "The Effect of Inlet Valve Timing and Engine Speed on Dual Fuel NG-Diesel Combustion in a Large Bore Engine," *SAE Int. J. Engines* 11, no. 2 (2018): 3-11, https://doi.org/10.4271/03-11-02-0015.
16. Xu, S., Anderson, D., Singh, A., Hoffman, M. et al., "Development of a Phenomenological Dual-Fuel Natural Gas Diesel Engine Simulation and Its Use for Analysis of Transient Operations," *SAE Int. J. Engines* 7, no. 4 (2014): 1665-1673, https://doi.org/10.4271/2014-01-2546.
17. Barro, C., Nani, C., Hutter, R., and Boulouchos, K., "Spray Model Based Phenomenological Combustion Description and Experimental Validation for a Dual Fuel Engine," SAE Technical Paper 2017-24-0098, 2017, https://doi.org/10.4271/2017-24-0098.
18. Nandagopal, S., Masimalai, S.K., and Krishnamurthy, K., "Data Driven Modeling of In-Cylinder Pressure of a Dual Fuel Compression Ignition Engine Operated with Renewable Fuels Using State Space Approach," SAE Technical Paper 2018-28-0022, 2018, https://doi.org/10.4271/2018-28-0022.
19. Zirngibl, S. and Wachtmeister, G., "Using a Phenomenological Simulation Approach for the Prediction of a Dual-Fuel Pilot Injection Combustion Process," SAE Technical Paper 2020-01-5013, 2020, https://doi.org/10.4271/2020-01-5013.
20. Taritas, I., Kozarac, D., Sjeric, M., Sierra Aznar, M. et al., "Development and Validation of a Quasi-Dimensional Dual Fuel (Diesel - Natural Gas) Combustion Model," *SAE Int. J. Engines* 10, no. 2 (2017): 483-500, https://doi.org/10.4271/2017-01-0517.
21. Krenn, M., Pirker, G., Wimmer, A., Djuranec, S. et al., "Methodology for Analysis and Simulation of Dual Fuel Combustion in Large Engines," in *THIESEL 2014 Conference Thermo- and Fluid Dynamic Processes in Direct Injection Engines*, Valencia (Spain), 1-14, 2014.
22. Morel, T. and Wahiduzzaman, S., "Modeling of Diesel Combustion and Emissions," in *XXVI FISITA Congress*, Prague (Czech Republic), 1996.
23. Jung, D. and Assanis, D.N., "Quasidimensional Modeling of Direct Injection Diesel Engine Nitric Oxide, Soot, and Unburned Hydrocarbon Emissions," *J. Eng. Gas Turbines Power* 128, no. 2 (2006): 388-396, https://doi.org/10.1115/1.2056027.
24. Musculus, M.P.B. and Kattke, K., "Entrainment Waves in Diesel Jets," *SAE Int. J. Engines* 2, no. 1 (2009): 1170-1193, https://doi.org/10.4271/2009-01-1355.
25. Zhou, X., Li, T., Lai, Z., and Wei, Y., "Modeling Diesel Spray Tip and Tail Penetrations after End-of-Injection," *Fuel* 237 (2019): 442-456, https://doi.org/10.1016/j.fuel.2018.10.029.
26. Livengood, J.C. and Wu, P.C., "Correlation of Autoignition Phenomena in Internal Combustion Engines and Rapid Compression Machines," *Symp. Combust.* 5, no. 1 (1955): 347-355, https://doi.org/10.1016/S0082-0784(55)80047-1.
27. Millo, F., Accurso, F., Piano, A., Caputo, G. et al., "Experimental and Numerical Investigation of the Ignition Process in a Large Bore Dual Fuel Engine," *Fuel* 290 (2021): 120073, https://doi.org/10.1016/j.fuel.2020.120073.
28. Ranzi, E., Frassoldati, A., Stagni, A., Pelucchi, M. et al., "Reduced Kinetic Schemes of Complex Reaction Systems: Fossil and Biomass-Derived Transportation Fuels," *International Journal of Chemial Kinetics* 46, no. 9 (2014): 512-542, https://doi.org/10.1002/kin.20867.
29. Kahila, H., Kaario, O., Ahmad, Z., Masouleh, M.G. et al., "A Large-Eddy Simulation Study on the Influence of Diesel Pilot Spray Quantity on Methane-Air Flame Initiation," *Combust. Flame* 206 (2019): 506-521, https://doi.org/10.1016/j.combustflame.2019.05.025.
30. Srna, A., Bolla, M., Wright, Y.M., Herrmann, K. et al., "Effect of Methane on Pilot-Fuel Auto-Ignition in Dual-Fuel Engines," *Proc. Combust. Inst.* 37, no. 4 (2019): 4741-4749, https://doi.org/10.1016/j.proci.2018.06.177.
31. Tekgül, B., Kahila, H., Kaario, O., and Vuorinen, V., "Large-Eddy Simulation of Dual-Fuel Spray Ignition at Different Ambient Temperatures," 215 (2020): 51-65, https://doi.org/10.1016/j.combustflame.2020.01.017.
32. Hardenberg, H.O. and Hase, F.W., "An Empirical Formula for Computing the Pressure Rise Delay of a Fuel from Its Cetane Number and from the Relevant Parameters of Direct-

Injection Diesel Engines," SAE Technical Paper 790493, 1979, https://doi.org/10.4271/790493.

33. Rether, D., Grill, M., Schmid, A., and Bargende, M., "Quasi-Dimensional Modeling of CI-Combustion with Multiple Pilot- and Post Injections," *SAE Int. J. Engines* 3, no. 1 (2010): 12-27, https://doi.org/10.4271/2010-01-0150.
34. Chmela, F.G., Pirker, G.H., and Wimmer, A., "Zero-Dimensional ROHR Simulation for DI Diesel Engines—A Generic Approach," *Energy Convers. Manag.* 48, no. 11 (2007): 2942-2950, https://doi.org/10.1016/j.enconman.2007.07.004.
35. Chmela, F., Engelmayer, M., Pirker, G., and Wimmer, A., "Prediction of Turbulence Controlled Combustion in Diesel Engines," in *Conference on Thermo- and Fluid Dynamic Processes in Diesel Engines*, Valencia (Spain), 1-15, 2004.
36. Wahiduzzaman, S., Moral, T., and Sheard, S., "Comparison of Measured and Predicted Combustion Characteristics of a Four-Valve S.I. Engine," SAE Technical Paper 930613, 1993, https://doi.org/10.4271/930613.
37. Fogla, N., Bybee, M., Mirzaeian, M., Millo, F. et al., "Development of a K-k-ε Phenomenological Model to Predict In-Cylinder Turbulence," *SAE Int. J. Engines* 10, no. 2 (2017): 1-14, https://doi.org/10.4271/2017-01-0542.
38. Metghalchi, M. and Keck, J.C., "Burning Velocities of Mixtures of Air with Methanol, Isooctane, and Indolene at High Pressure and Temperature," *Combust. Flame* 48, no. C (1982): 191-210, https://doi.org/10.1016/0010-2180(82)90127-4.
39. Gülder, O.L., "Burning Velocities of Ethanol-Air and Ethanol-Water-Air Mixtures," AIAA Progr Astronaut Aeronaut 95 (1984): 181-197.
40. Amirante, R., Distaso, E., Tamburrano, P., and Reitz, R.D., "Laminar Flame Speed Correlations for Methane, Ethane, Propane and Their Mixtures, and Natural Gas and Gasoline for Spark-Ignition Engine Simulations," *Int. J. Engine Res.* 18, no. 9 (2017): 951-970, https://doi.org/10.1177/1468087417720018.
41. Wang, Y., Movaghar, A., Wang, Z., Liu, Z. et al., "Laminar Flame Speeds of Methane/Air Mixtures at Engine Conditions: Performance of Different Kinetic Models and Power-Law Correlations," *Combust. Flame* 218 (2020): 101-108, https://doi.org/10.1016/j.combustflame.2020.05.004.
42. Masouleh, M.G., Wehrfritz, A., Kaario, O., Kahila, H. et al., "Comparative Study on Chemical Kinetic Schemes for Dual-Fuel Combustion of n-Dodecane/Methane Blends," *Fuel* 191 (2017): 62-76, https://doi.org/10.1016/j.fuel.2016.10.114.
43. Smith, G.P., Golden, D.M., Frenklach, M., Moriarty, N.W. et al., "GRI-Mech 3.0," http://combustion.berkeley.edu/gri-mech/version30/text30.html, accessed 22 December 2021.
44. Wang, H., You, X., Joshi, A.V., Davis, S.G. et al., "USC Mech Version II. High-Temperature Combustion Reaction Model of H2/CO/C1-C4 Compounds," May 2007, http://ignis.usc.edu/Mechanisms/USC-Mech%20II/USC_Mech%20II.htm, accessed 22 December 2021.
45. Narayanaswamy, K., Pepiot, P., and Pitsch, H., "A Chemical Mechanism for Low to High Temperature Oxidation of n-Dodecane as a Component of Transportation Fuel Surrogates," *Combust. Flame* 161, no. 4 (2014): 866-884, https://doi.org/10.1016/j.combustflame.2013.10.012.
46. García Valladolid, P., Tunestål, P., Monsalve-Serrano, J., García, A. et al., "Impact of Diesel Pilot Distribution on the Ignition Process of a Dual Fuel Medium Speed Marine Engine," *Energy Convers. Manag.* 149, no. 2017 (2017): 192-205, https://doi.org/10.1016/j.enconman.2017.07.023.
47. Eder, L., Kiesling, C., Priesching, P., Pirker, G. et al., "Multidimensional Modeling of Injection and Combustion Phenomena in a Diesel Ignited Gas Engine," SAE Technical Paper 2017-01-0559, 2017, https://doi.org/10.4271/2017-01-0559.
48. Burke, E.M., Güthe, F., and Monaghan, R.F.D., "A Comparison of Turbulent Flame Speed Correlations for," in *Proceedings of the ASME Turbo Expo 2016 Turbomachinery Technical Conference Expo*, Seoul (South Korea), 1-13, 2016.
49. Reddy Muppala, S.P., Aluri, N.K., Dinkelacker, F., and Leipertz, A., "Development of an Algebraic Reaction Rate Closure for the Numerical Calculation of Turbulent Premixed Methane, Ethylene, and Propane/Air Flames for Pressures up to 1.0 MPa," *Combust. Flame* 140, no. 4 (2005): 257-266, https://doi.org/10.1016/j.combustflame.2004.11.005.
50. Kobayashi, H., "Experimental Study of High-Pressure Turbulent Premixed Flames," *Exp. Therm. Fluid Sci.* 26, no. 2-4 (2002): 375-387, https://doi.org/10.1016/S0894-1777(02)00149-8.
51. Ratzke, A., Schöffler, T., Kuppa, K., and Dinkelacker, F., "Validation of Turbulent Flame Speed Models for Methane-Air-Mixtures at High Pressure Gas Engine Conditions," *Combust. Flame* 162, no. 7 (2015): 2778-2787, https://doi.org/10.1016/j.combustflame.2015.04.011.
52. Morel, T., Rackmil, C.I., Keribar, R., and Jennings, M.J., "Model for Heat Transfer and Combustion in Spark Ignited Engines and Its Comparison with Experiments," SAE Technical Paper 880198, 1988, https://doi.org/10.4271/880198.
53. Walther, H.-P., Schlatter, S., Wachtmeister, G., and Boulouchos, K., "Combustion Models for Lean-Burn Gas Engines with Pilot Injection," *MTZ Worldw.* 73, no. 2 (2012): 56-63, https://doi.org/10.1365/s38313-012-0144-3.
54. Lavole, G.A., Heywood, J.B., and Keck, J.C., "Experimental and Theoretical Study of Nitric Oxide Formation in Internal Combustion Engines," *Combust. Sci. Technol.* 1, no. 4 (1970): 313-326, https://doi.org/10.1080/00102206908952211.
55. Millo, F., Boccardo, G., Piano, A., Arnone, L. et al., "Numerical Simulation of the Combustion Process of a High EGR, High Injection Pressure, Heavy Duty Diesel Engine," SAE Technical Paper 2017-24-0009, 2017, https://doi.org/10.4271/2017-24-0009.